inter·noise 2021
1–5 August | Washington, DC

Equation Chapter 1 Section 1

Comparison of two community noise models applied to a NASA urban air mobility concept vehicle

Stephen A. Rizzi[1]
Aeroacoustics Branch, NASA Langley Research Center
Hampton, VA 23681-2199, USA

Juliet A. Page[2]
Volpe National Transportation Systems Center, 55 Broadway
Cambridge, MA 02142-1093, USA

Rui Cheng[3]
National Institute of Aerospace, 100 Exploration Way
Hampton, VA 23666-6266, USA

ABSTRACT

Predictions of community noise exposure from a NASA urban air mobility (UAM) concept vehicle have been conducted for representative operations using the FAA Aviation Environmental Design Tool (AEDT) in order to demonstrate modeling tool interoperability and assess applicability, capabilities and limitations of integrated noise modeling tools. To both quantify limitations and highlight other capabilities, a comparative analysis is performed using a time-domain simulation method, in particular, using the Volpe Advanced Acoustic Model (AAM). Using the same source noise model, the 3D directivity of a UAM concept vehicle is predicted in terms of aeroacoustic pressure time histories at a sphere of observer positions near the vehicle. In addition to distilling those data to a set of noise-power-distance data for input to AEDT, the data are processed preserving spectral directivity, into one-third and one-twelfth octave bands for input to AAM. Results from AEDT and AAM modeling are provided for a variety of metrics to demonstrate the effect that source noise directivity and propagation modeling fidelity have on predicted results at receptors over a study area.

1. INTRODUCTION

A comparative analysis was conducted with the FAA's Aviation Environmental Design Tool (AEDT) [1] and the Volpe Advanced Acoustic Model (AAM) [2] for the purposes of assessing modeling applicability, capabilities and limitations, and identifying potential future modeling

[1] stephen.a.rizzi@nasa.gov
[2] juliet.page@dot.gov
[3] rui.cheng@nasa.gov

improvements. AEDT is an integrated model developed for assessing cumulative noise impacts from aviation noise sources. It includes vehicle source directivity adequate for assessing fixed-wing and conventional rotary-wing community noise, but has limited ability for considering complex advanced air mobility configurations. A set of noise spheres with full three-dimensional spectral directivity in one-third octave band and one-twelfth octave bands was modeled for a NASA quadrotor reference vehicle. These noise spheres were used to model a selected flight operation in AAM to benchmark A-weighted metric results on ground contours and points of interest for the purposes of comparison with AEDT. Derivative omnidirectional and axisymmetric noise spheres were also developed to evaluate the impact of limited directivity assumptions. Some advanced AAM analyses using acoustic visualization, narrow band analysis and calculation of time varying loudness metrics were conducted to aid in interpreting acoustic results.

2. CONCEPT VEHICLES, TRAJECTORIES, AND OPERATING STATES

2.1. Vehicle Descriptions

Noise from the quadrotor reference vehicle developed under the NASA Revolutionary Vertical Lift Technology (RVLT) Project was investigated in this paper, see Figure 1. The vehicle was sized for a 1200 lb. payload (up to six passengers) executing a representative mission profile [3]. The quadrotor was an all-electric variant, with three-bladed rotors, gross weight of 6469 lb., and maximum airspeed V_{max} of 109 knots true airspeed (KTAS). Additional details on this configuration can be found in Ref. [4].

2.2. Trajectory Data

Trajectory data were generated using a mission planner algorithm developed by NASA for UAM operations research [5]. The route data are the same as those used in the X2 engineering evaluation conducted by the NASA Air Traffic Management – Exploration (ATM-X) Project, UAM subproject. The X2 evaluation consisted of sixteen routes in the Dallas-Ft. Worth, TX, area. The maximum airspeed was limited to 85% of V_{max}.

2.3. Determination of Operating States

The trajectory data were reduced to determine aircraft operational states for which noise estimates are needed, see Section 3. In this paper, the aircraft operational states are defined by pairs of airspeed (knots) and climb angle (deg.). It was considered impractical to generate noise estimates based on 1 Hz trajectory data for each of the sixteen routes. A condensation scheme was developed to select operational states based on the number of occurrences (counts) over sixteen routes [6]. This resulted in 42 unique operating states, as shown in Figure 2. A unique numerical identifier, e.g., 101, 102, etc., was used to identify the particular operating state.

3. SOURCE NOISE DATA GENERATION

This section describes the process for generating user-defined source noise sphere data through analysis. The process involves two steps; the first step determines the trimmed condition at each operating state and the second step performs the acoustic analysis. A summary of each step follows. The overall process, depicted in Figure 3, is a subset of that used to generate noise-power-distance (NPD) data for input to AEDT [6].

3.1. Vehicle Trim

Given the vehicle configuration and prescribed operating state, the vehicle is “trimmed” in an iterative fashion using a comprehensive analysis code. In the trimmed condition, the control surface configuration of the vehicle corresponds to the desired flight condition. For this work, the Comprehensive Analytical Model of Rotorcraft Aerodynamics and Dynamics (CAMRAD II) [7] was used to trim the vehicle.

Figure 1: NASA RVLT quadrotor reference vehicle configuration considered in this study.

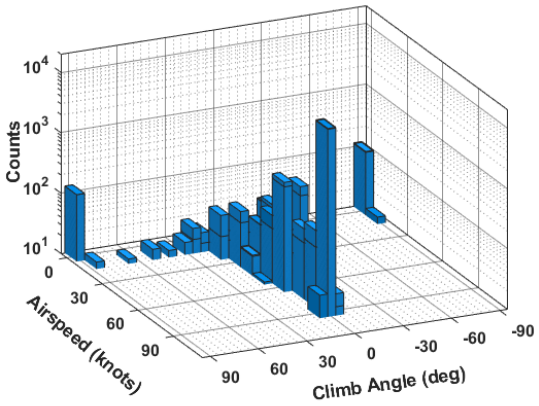

Figure 2: Operating states for the quadrotor reference vehicle.

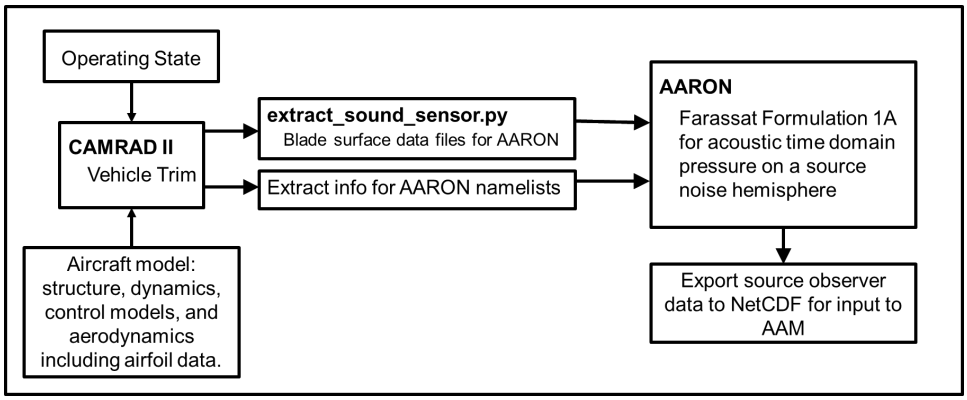

Figure 3: NASA process for generating source noise data for input to AAM.

The rotors on the quadrotor vehicle operate at a constant RPM with a 20 Hz blade passage frequency (BPF) and utilize collective pitch control. The trim targets are the six degrees-of-freedom (F_x, F_y, F_z, M_x, M_y, and M_z), and trim variables include four collective control combinations of rotor pairs, plus vehicle pitch and roll. The same trim mode was used at all speeds.

3.2. Source Noise Spheres

The resulting blade loadings and motion from the trim operation serve as input to a system noise prediction. In this work, the ANOPP2 Aeroacoustic ROtor Noise (AARON) tool, a part of the NASA 2nd generation Aircraft Noise Prediction Program (ANOPP2) [8], was used for the system noise prediction. The acoustics solver uses Farassat's Formulation F1A [9] to compute the periodic loading and thickness noise components under a quasistatic operating condition at a set of observers at a fixed radius from the aircraft center of gravity. The set of observers constitutes the source noise sphere and the two noise components included constitute the so-called first generation (Gen 1.2) database. Although only the lower hemisphere of observers (below the vehicle) was computed in this work, the more general sphere usage is retained. Each source noise sphere (one for each operating state) is exported as one-third and one-twelfth octave band data to a NetCDF file for input to AAM. Per AAM compact source modeling requirements, noise spheres are referenced to a finite radius. Spectral data on the noise sphere were provided on a spherical coordinate system mesh with 10° spacing. The polar angle, θ, ranges from 0° at the nose to 180° at the tail, while the azimuth angle, ϕ, ranges from -90° on the port (left) side to +90° on the starboard (right) side.

Sample source noise data in the form of one-third octave band sound pressure levels (SPL) are shown in Figure 4 for a low speed ascent condition (10 knot airspeed and 85° climb angle) and high speed descent condition (60 knot airspeed and -5° climb angle), and in the left-hand side of Figure 5 for a high speed cruise condition (90 knot airspeed and 0° climb angle). The data represent the 20 Hz one-third octave band incorporating the BPF. The higher levels for the high speed descent condition are due to the presence of blade-vortex interaction noise, as evidenced by blade loading data (not shown). The source data may be highly directional, as also evidenced by the overall SPL on the right-hand side of Figure 5. In contrast, the NPD used in the companion AEDT analyses are derived from source data along the centerline (0° azimuth), with an assumed 90° dipole directivity used in the noise fraction adjustment for fixed-wing aircraft. Consequently, AAM and AEDT predictions are expected to best agree under the flight track, and differ at lateral locations due, in part, to differences in source spectral directivity.

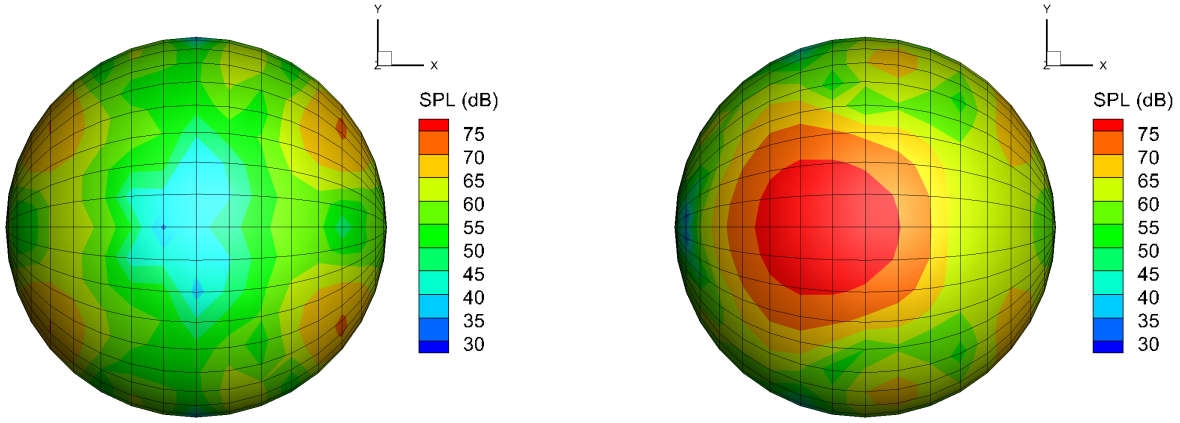

Figure 4: Source noise data for low speed ascent (left) and high speed descent (right) conditions in the 20 Hz one-third octave band. Nose is in the positive x-direction.

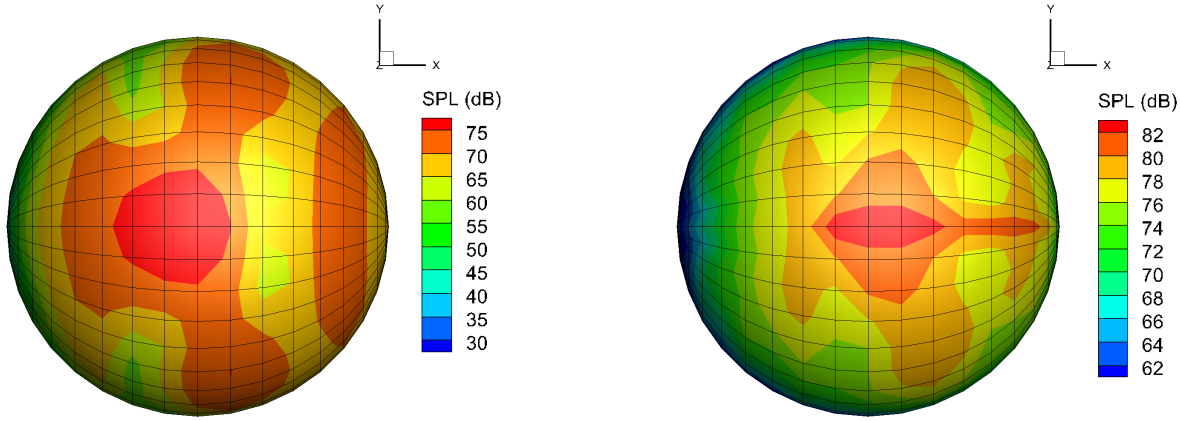

Figure 5: Source noise data for high speed cruise condition in the 20 Hz one-third octave band (left) and the overall sound pressure level (right). Nose is in the positive x-direction.

The NPD values for A-weighted sound exposure level (SELA) and maximum A-weighted sound pressure level (LmaxA) used in the AEDT analyses were computed using the 3D noise spheres, see companion paper [6] for details. Azimuthal source directivity was not directly accounted for because the AEDT analyses were performed using a fixed-point flight profile method for fixed-wing propeller aircraft. Consequently, the NPD values reflected only the polar spectral directivity along the 0° azimuth, versus a better representation of azimuthal directivity that could be achieved using AEDT helicopter modes or the full 3D directivity in AAM using the ANOPP2 sphere.

4. AAM MODELING

4.1. Trajectory Data

AAM input trajectory data were developed from the combination of AEDT track and profile point data specified in the companion paper [6]. Using the NCSPEC option for AAM input, each trajectory point consisted of x and y coordinates in Universal Transverse Mercator (UTM) coordinates, the altitude, airspeed, operating state identifier (via AAM keyword NCSPEC), and other parameters related to the attitude of the aircraft. The latter were set to model level flight as the aircraft attitude was already reflected in the source noise sphere data. In AAM, additional simulation time steps were interpolated from the input trajectory in order to achieve at least 0.5 sec time spacing. In using the NCSPEC option, AAM utilizes a constant noise source between simulation points; however, AAM will interpolate on speed when developing the simulation trajectory. To limit that, a 'guard' track point, having the same operating state identifier and speed as the previous track point, is inserted just prior to the next input trajectory point. In doing so, interpolation of speed is limited to a short (12 ft.) transition segment. To the maximum extent possible, this replicated the conditions under which the AEDT analyses were performed using a fixed-point flight profile methodology outlined in the companion paper.

4.2. Calibration of Noise Spheres for AAM

A calibration process is utilized in order to account for differences in the AAM and AEDT propagation models. A reference trajectory was chosen based on the most prevalent cruising condition, namely 90 knots level flight at 1000 ft. altitude. An idealized trajectory at the reference condition was developed in AEDT and the undertrack centerline LmaxA was calculated using the NPD data [6]. The corresponding noise sphere was analyzed in AAM and a spectrally uniform calibration factor was applied over the entire sphere so that LmaxA predictions matched between AAM and AEDT. The resulting calibration factors (see below) were found to be very small. AEDT results are reported for grid receptors at 4 ft. above ground level (AGL) and a corresponding 4 ft. AGL height was used for AAM Points of Interest (POIs) with a matched slant range (1000 ft.) between the source and receiver at the point of closest approach (directly overhead).

Three different noise spheres were generated using derivative information from the analysis described in the companion paper [6] and calibrated using the reference trajectory. These spheres include:

- Omnidirectional – undertrack spectra at the point of LmaxA repeated in all directions (Figure 6, Calibration: +0.33 dB)
- Axisymmetric – undertrack polar spectral directivity repeated at all azimuthal angles (Figure 7, Calibration: +0.21 dB)
- Full 3D – based on the ANOPP2-based modeling described in Section 3.2 (as shown uncalibrated on the right-hand side of Figure 5, Calibration: +0.21 dB)

4.3. Comparison of AEDT with AAM Omnidirectional Sphere Results at Lateral POIs

The reference case described in Section 4.2 was modeled in AEDT and AAM. Results (SELA and LmaxA) were predicted at a series of receptors undertrack and at lateral distances of 500, 1000, 2000, 3000, 4000 and 5000 ft. and compared using the calibrated omnidirectional, axisymmetric and 3D spheres. Table 1 lists the POIs and the corresponding sphere angles.

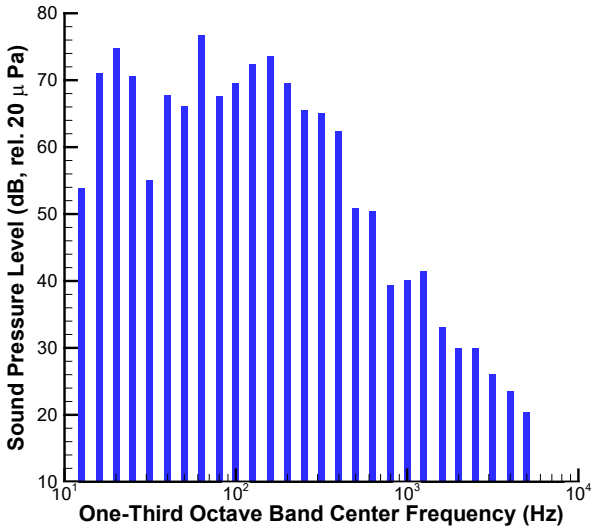

Figure 6: Quadcopter spectrum for 90 kt level flight for omnidirectional sphere (calibrated).

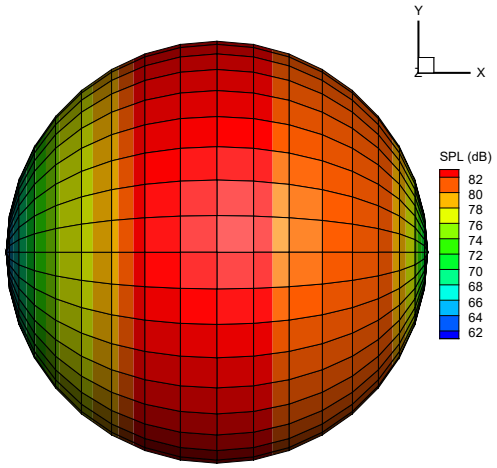

Figure 7: Axisymmetric sphere (unweighted), 90 kt level flight (calibrated). Nose to right.

Table 1: AAM sphere geometric information at points corresponding to LmaxA at the POIs.

	Geometry for LmaxA			
Receiver	**Lateral Dist (ft.)**	**Phi (deg)**	**Theta (deg)**	**Slant Range (ft.)**
1	0	0	79	1019
2	500	-27	70	1194
3	1000	-45	61	1624
4	2000	-63	50	2909
5	3000	-72	50	4107
6	4000	-76	80	4186
7	5000	-79	60	5878

AAM Omnidirectional Sphere

Since the sphere calibration was conducted for LmaxA for a 1000 ft. slant range, directly undertrack, these predictions are identical (Figure 8, AEDT: red, AAM: black) at that range. The SELA values differ by 1.7 dB and this is attributable to polar spectral directivity that accumulates in the SELA calculation. The NPD generation analysis was based on a slice of the 3D sphere along the centerline (right-hand side of Figure 5) which exhibits considerable variation from nose to tail, whereas the AAM analysis utilizes a single spectrum in all directions on the sphere (Figure 6). The SELA metric is computed from the full time history (within 10 dB of the maximum) while the LmaxA metric is only matched at the peak of the time history.

Comparison of AEDT with AAM Axisymmetric Sphere Results at Lateral POIs

For the case where AEDT lateral results are compared with the AAM axisymmetric results (Figure 9), the undertrack levels at 1000 ft. for both SELA and LmaxA are identical due to the consistency in the polar directivity for the two models. For other lateral locations, slight differences are noted and are due to different propagation models used in AAM and AEDT. The AEDT analysis modeled the vehicle as a propeller aircraft, which does not include azimuthal source directivity, and is functionally equivalent to the AAM axisymmetric sphere. Note that AAM includes a more sophisticated ground effects model than AEDT that considers direct and reflected rays and can exhibit significant ‘dips’ in the received sound spectrum.

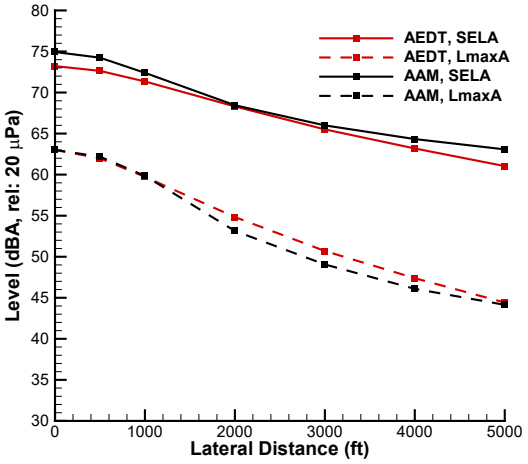

Figure 8: Metric comparison AEDT vs. AAM (omnidirectional sphere) at lateral POIs.

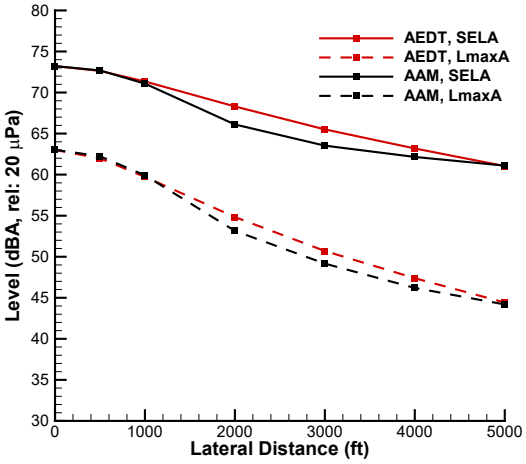

Figure 9: Metric comparison AEDT vs. AAM (axisymmetric sphere) at lateral POIs.

Comparison of AEDT with AAM 3D Sphere Results at Lateral POIs

Significant differences in the metric prediction at lateral positions are evident between AAM and AEDT when using the 3D spheres (Figure 10). This is primarily due to differences in azimuthal directivity and provides an example of potential differences between simplified source modeling for fixed-wing aircraft in AEDT and 3D sources in AAM.

Examination of AAM Time Histories at Lateral POIs

The A-weighted sound pressure level time history is provided in Figures 11 and 12 for the undertrack and 3000 ft. lateral POIs, respectively. Figure 11 shows a comparison of the time history at the undertrack POI between the three spheres, where the differences in polar directivity are evident. The axisymmetric and 3D sphere results align perfectly for the entire time history as expected, since the axisymmetric sphere was developed from the 3D centerline polar spectral directivity.

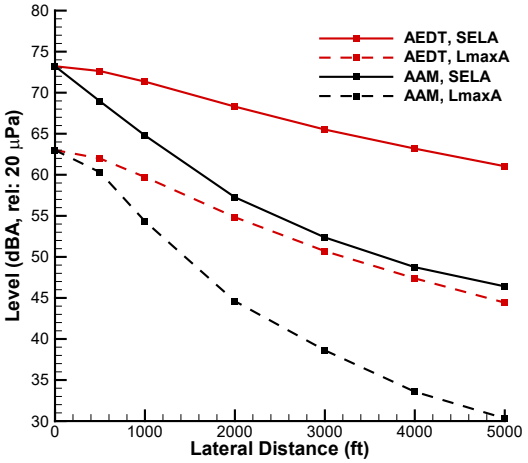

Figure 10: Metric comparison AEDT vs. AAM (3D sphere) at lateral POIs.

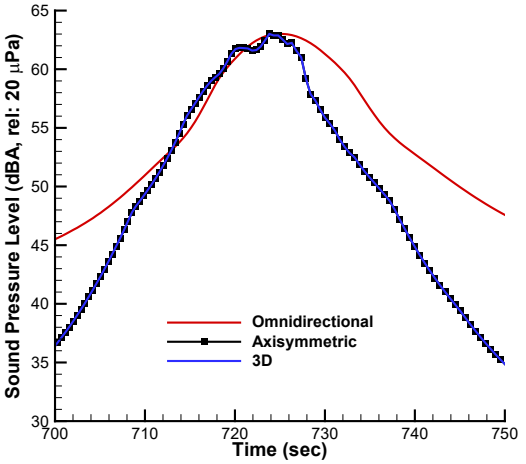

Figure 11: AAM undertrack sound pressure level time histories for 3 calibrated spheres.

At the 3000 ft. lateral POI location (Figure 12), one can see significant amplitude and shape differences throughout the time history. Differences in polar directivity for the 3D and axisymmetric spheres results in LmaxA occurring at different times. The differences in the LmaxA levels are also reflected in Figure 10 at the 3000 ft. lateral location. The unsteadiness in the time history traces in Figure 11 and Figure 12 is due to ground effects for the 4 ft. receiver height. This

behavior is also evident in the selected time history bands for the 3D sphere at the undertrack location, as shown in Figure 13.

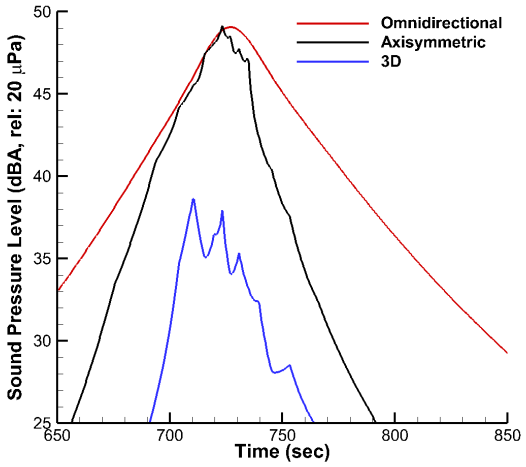

Figure 12: AAM sideline sound pressure level time histories for 3 calibrated spheres.

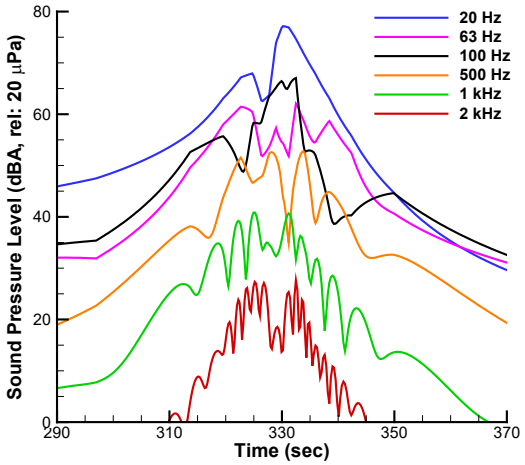

Figure 13: AAM undertrack one-third octave band sound pressure level time histories for calibrated 3D sphere.

5. SAMPLE RESULTS

5.1. AAM and AEDT Analysis for a Selected Operation

One of sixteen routes, KCAT-KDT4 [6], was selected for an in-depth analysis using AAM in order to illustrate and compare analyses results and provide visual insight. The spheres used in this section were calibrated using the process described in Section 4.2. The same calibration factor, based on the 90 kts level flight condition, was used for each of the 42 quadcopter spheres prior to AAM analysis. This was done to reduce complexity and scope. However, one could also calibrate each of the other flight condition spheres individually using a similar process.

5.2. Metric Comparison at Points of Interest near Takeoff and Landing Sites

Four series of points were identified for comparison of metrics between AEDT and AAM, see Figure 14. Each includes one undertrack location and six lateral locations up to 5000 ft. sideline ground distance. Figure 15 shows the 'Cruz' POIs areas in the takeoff and landing regions. The AEDT overpredictions, compared with the AAM simulations using the full 3D source directivity, are consistent with those in the reference case described in Section 4.3.

5.3. Contour Comparison

AEDT and AAM contours of LmaxA and SELA are provided in Figures 16 and 17, respectively. One can see that the LmaxA contours from AEDT in the vicinity of vertiports are nearly circular as the source is essentially a monopole. In contrast, the LmaxA contours from AAM reflect the more complex directivity character. Likewise, the SELA contours from AEDT (Figure 17) reflect the simplified 90 deg. dipole used in the AEDT noise fraction calculation for fixed-wing aircraft, whereas those from AAM exhibit the true 3D directivity with lower levels at lateral locations. Both sets of results compare favorably under the track, but increasingly differ away from the track, in part due to the previously noted lateral attenuation differences between AEDT and AAM. The abrupt transitions between spheres are seen in the AAM results since the NCSPEC keyword does not allow interpolation between different spheres.

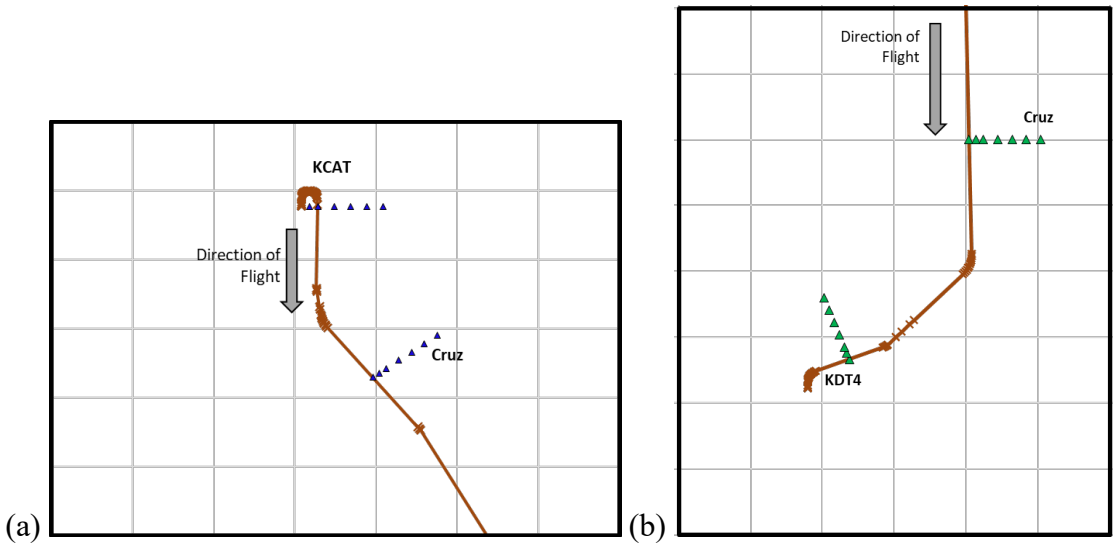

Figure 14: Flight track and points of interest near the KCAT-KDT4 takeoff region (a) and landing region (b) with 5000 ft. grid spacing indicated.

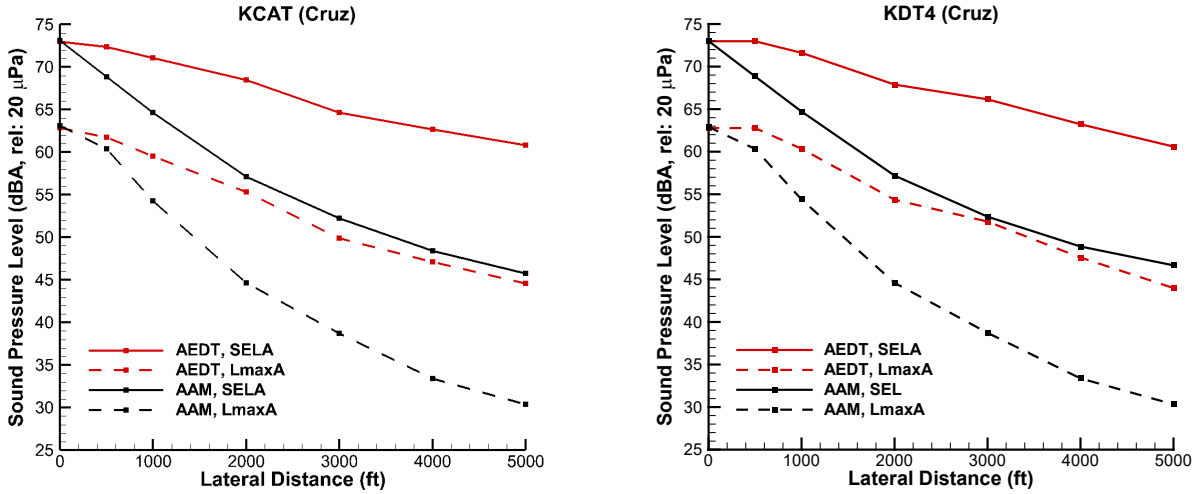

Figure 15: Metric comparisons for 'Cruz' POIs near takeoff (left) and landing (right) regions.

5.4. Acoustic Simulation Visualization using AAM

AAM can be used to create animations in a variety of metrics and individual one-third or one-twelfth octave bands, in order to visualize acoustic influences of vehicle directivity and transition segments, and to assess impacts on the ground. Acoustic visualization is also helpful to understand specific features seen in spectral time histories. The instantaneous LmaxA footprint illustrated in Figure 18 (a) is from a point where the vehicle passes over the takeoff cruise points of interest near KCAT. The swirling is due to differences in arrival times for various portions of the directivity pattern emitted at different heading angles. Figure 18 (b) illustrates the 20 Hz one-third octave band later in the cruise portion of the trajectory (shortly after the vehicle has passed over the approach POI). Note the clear indication of the lobes in the directivity pattern, including those aft of the vehicle. When viewing the acoustic animations (available for download [10, 11]), transitions between operating modes are apparent, and can aid in the design of operational procedures as well as in the understanding of how 3D spectral directivity data affect auralized sounds, such as those from the NASA Auralization Framework [12].

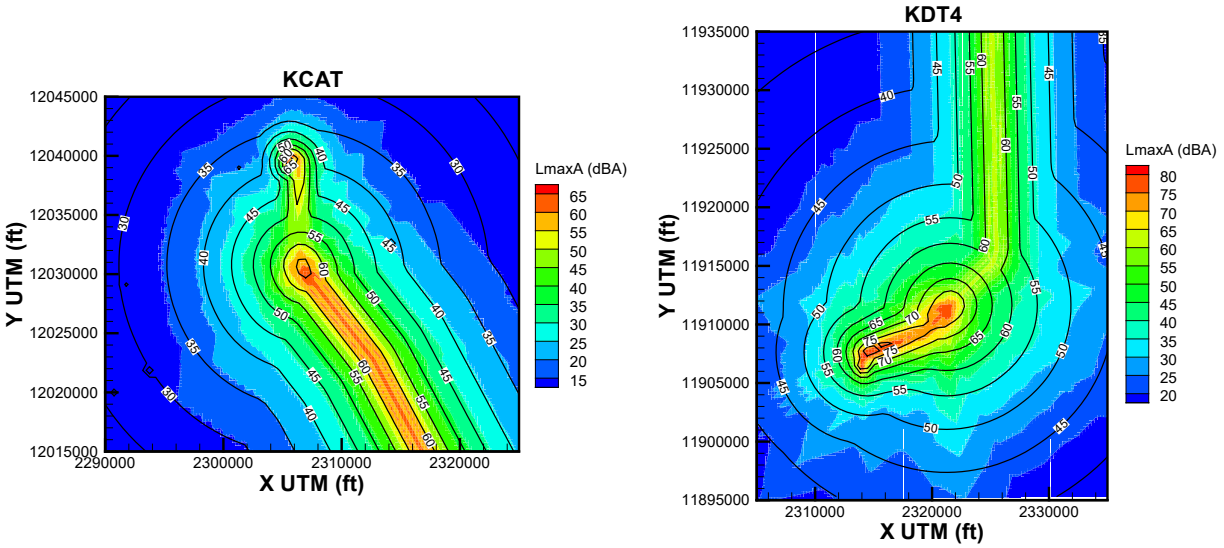

Figure 16: Comparison of AEDT (lines) and AAM (color fill) LmaxA contours in the takeoff (left) and landing (right) areas over the calculation region identified in Figure 14.

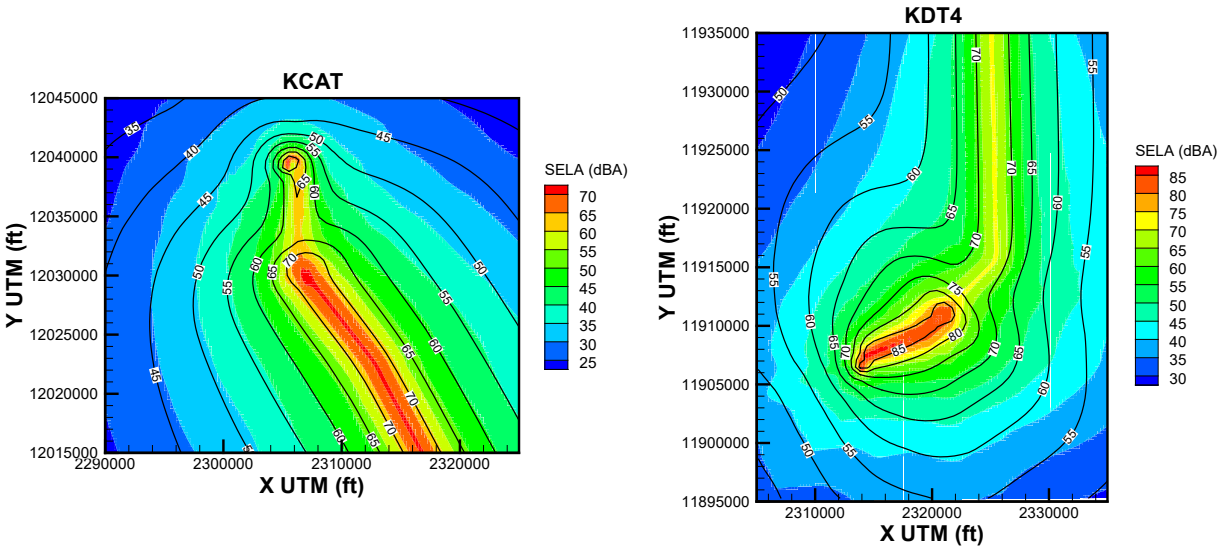

Figure 17: Comparison of AEDT (lines) and AAM (color fill) SELA contours in the takeoff (left) and landing (right) areas over the calculation region identified in Figure 14.

5.5. Advanced Analyses using AAM

Additional capabilities have been recently added to AAM to facilitate in-depth analysis of advanced air mobility vehicle operations; including computation of time varying loudness (TVL) metrics in the presence of background noise spectra, instantaneous loudness (sone), short term (ST) and long term (LT) loudness (sone), d' (d prime), and long term loudness level (phon) from one-third or one-twelfth octave bands [13, 14]. In this example, the same KCAT-KDT4 operation was examined using calibrated one-twelfth octave band noise spheres. Empirical ambient noise spectra [15] obtained in the Dallas area for the morning rush hour and in the quiet nighttime were used to assess TVL for the POIs under consideration. An example TVL time history for a point at 500 ft. sideline to the cruise-approach transition in Figure 19 illustrates multiple peaks near the point of closest approach. In this demonstration, the values of d' indicate that the vehicle would be audible during the nighttime, but not in the daytime. Examination of the footprint in Figure 19 suggests that the directivity lobes are responsible for these details. Although the quadrotor vehicle

noise spheres include only loading and thickness noise and the trajectories are simplified and not optimized, these advanced analysis capabilities can aid the vehicle and operational route designer.

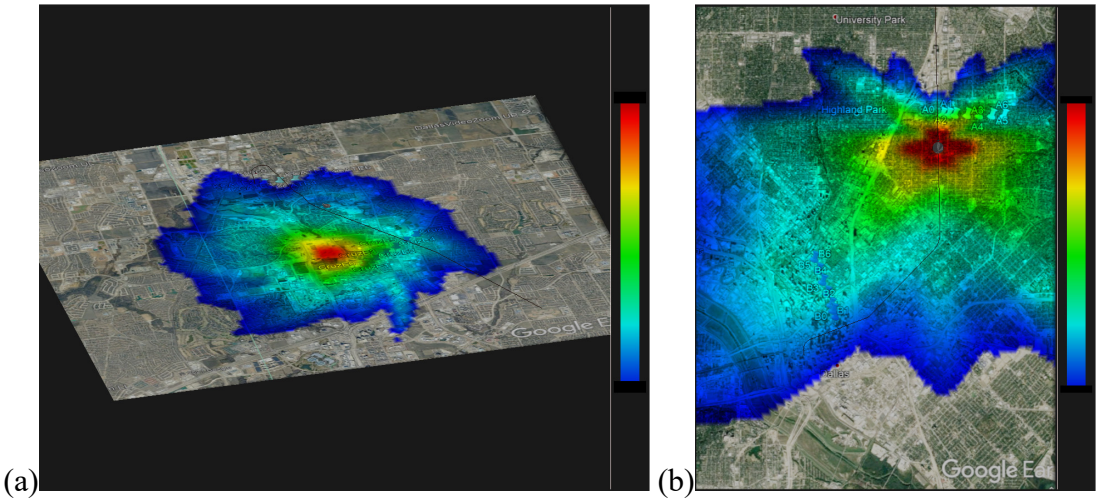

Figure 18: AAM temporally interpolated instantaneous ground receiver levels using 3D calibrated spheres at two locations for the KCAT-KDT4 operation.

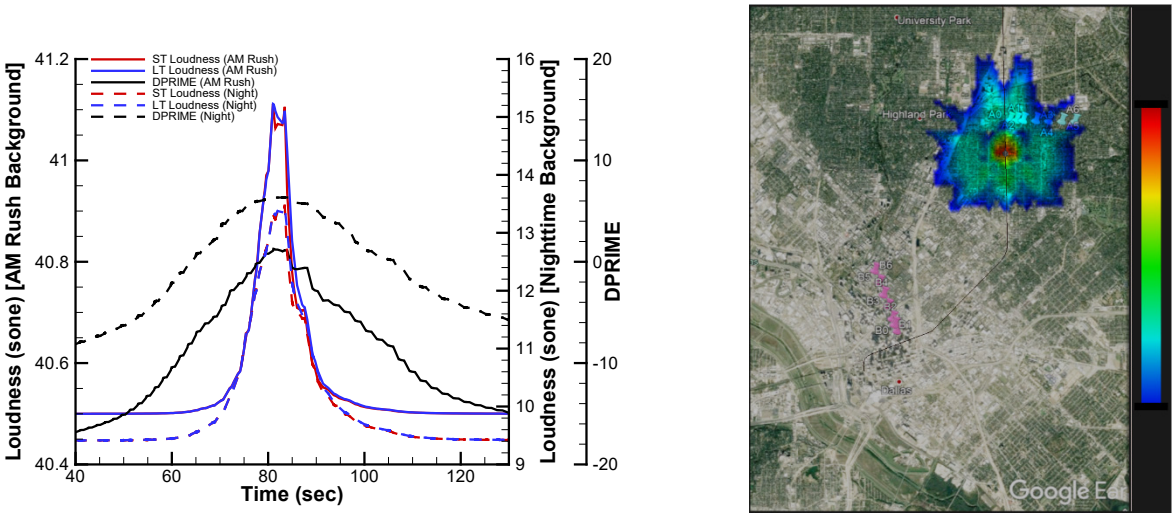

Figure 19: Computed TVL metrics at a 500 ft. sideline POI near the cruise-approach transition (left) and the 100 Hz footprint for a time just after the vehicle has passed over this POI (right).

6. CONCLUDING REMARKS

Comparative analyses between AEDT and AAM suggest that 3D spectral directivity can be an important feature to capture, particularly at lateral locations. However, these observations are based on data that do not include broadband noise, which may dominate at higher frequencies and result in a more uniform directivity. Subsequent noise generation data, containing broadband self noise, may be used to assess that possibility. Acoustic visualization tools can be used to assess impacts of 3D spectral directivity and the influence of operational procedure design. Time varying loudness metrics can be assessed against differing backgrounds at points of interest or over a grid. Future plans include an evaluation of the helicopter modeling capability within AEDT, which will allow right-center-left directivity to be incorporated in the analyses, and demonstrating the feasibility of developing visualization and auralization from a common analysis. Long term AAM

development plans include the development of automated sphere selection and interpolation procedures for advanced air vehicles.

7. ACKNOWLEDGMENTS

This work was partially supported by the NASA Aeronautics Research Mission Directorate, Revolutionary Vertical Lift Technology Project. The authors wish to acknowledge Doug Boyd (NASA Langley) for the AARON tool development and assistance in generating source noise spheres.

8. REFERENCES

1. "Aviation Environmental Design Tool (AEDT) technical manual, Version 3c," U.S. Department of Transportation, Volpe National Transportation Systems Center, Cambridge, MA, DOT-VNTSC-FAA-20-05, 2020.
2. "Advanced Acoustic Model (AAM), Technical Reference and User's Guide," U.S. Department of Transportation, Volpe National Transportation Systems Center, Cambridge, MA, DOT-VNTSC-20-05, 2020.
3. Patterson, M.D., Antcliff, K.R., and Kohlman, L.W., "A proposed approach to studying urban air mobility missions including an initial exploration of mission requirements," *AHS International 74th Annual Forum and Technology Display*, Phoenix, AZ, 2018.
4. Silva, C., Johnson, W.R., Solis, E., Patterson, M.D., and Antcliff, K.R., "VTOL urban air mobility concept vehicles for technology development," *AIAA AVIATION Forum*, AIAA-2018-3847, Atlanta, GA, 2018.
5. Guerreiro, N.M., Butler, R.W., Maddalon, J.M., and Hagen, G.E., "Mission planner algorithm for urban air mobility – Initial performance characterization," *AIAA AVIATION Forum*, AIAA-2019-3626, Dallas, TX, 2019.
6. Rizzi, S.A. and Rafaelof, M., "Community noise assessment of urban air mobility vehicle operations using the FAA Aviation Environmental Design Tool," *InterNoise 2021*, Virtual Meeting, 2021.
7. Johnson, W.R., "Rotorcraft aerodynamic models for a comprehensive analysis," *AHS International 54th Annual Forum*, Washington, DC, 1998.
8. Lopes, L.V. and Burley, C.L., "ANOPP2 User's Manual: Version 1.2," NASA TM-2016-219342, 2016.
9. Farassat, F. and Succi, G., "The prediction of helicopter rotor discrete frequency noise," *Vertica*, Vol. 7, pp. 309-320, 1983.
10. "Aircraft flyover simulation," NASA, https://stabserv.larc.nasa.gov/flyover/, 2021.
11. "Advanced Acoustic Model (AAM) software," U.S. DOT Volpe Center, https://www.volpe.dot.gov/AAM, 2021.
12. Aumann, A.R., Tuttle, B.C., Chapin, W.L., and Rizzi, S.A., "The NASA Auralization Framework and plugin architecture," *InterNoise 2015*, San Francisco, CA, 2015.
13. Moore, B.C.J., Glasberg, B.R., Varathanathan, A., and Schlittenlacher, J., "A loudness model for time-varying sounds incorporating binaural inhibition," *Trends in Hearing*, Vol. 20, 2016.
14. Moore, B.C.J., Jervis, M., Harries, L., and Schlittenlacher, J., "Testing and refining a loudness model for time-varying sounds incorporating binaural inhibition," *The Journal of the Acoustical Society of America*, Vol. 143, No. 3, pp. 1504-1513, 2018.
15. Page, J.A., "Modeling noise and acceptability of eVTOL operations," *Uber Elevate Summit*, 2018.